Sir2 Protein Deacetylases: Evidence for Chemical Intermediates and Functions of a Conserved Histidine†

Brian C. Smith‡ and John M. Denu*,§

Departments of Biomolecular Chemistry and Chemistry, University of Wisconsin—Madison, Madison, Wisconsin 53706

Received October 4, 2005; Revised Manuscript Received November 2, 2005

ABSTRACT: Sir2 NAD^+-dependent protein deacetylases are implicated in a variety of cellular processes such as apoptosis, gene silencing, life-span regulation, and fatty acid metabolism. Despite this, there have been relatively few investigations into the detailed chemical mechanism. Sir2 proteins (sirtuins) catalyze the chemical conversion of NAD^+ and acetylated lysine to nicotinamide, deacetylated lysine, and 2′-*O*-acetyl-ADP-ribose (*O*AADPr). In this study, Sir2-catalyzed reactions are shown to transfer an ^{18}O label from the peptide acetyl group to the ribose 1′-position of *O*AADPr, providing direct evidence for the formation of a covalent α-1′-*O*-alkylamidate, whose existence is further supported by the observed methanolysis of the α-1′-*O*-alkylamidate intermediate to yield *β*-1′-*O*-methyl-ADP-ribose in a Sir2 histidine-to-alanine mutant. This conserved histidine (His-135 in HST2) activates the ribose 2′-hydroxyl for attack on the α-1′-*O*-alkylamidate. The histidine mutant is stalled at the intermediate, allowing water and other alcohols to compete kinetically with the attacking 2′-hydroxyl. Measurement of the pH dependence of k_{cat} and k_{cat}/K_m values for both wild-type and histidine-to-alanine mutant enzymes confirms roles of this residue in NAD^+ binding and in general-base activation of the 2′-hydroxyl. Also, transfer of an ^{18}O label from water to the carbonyl oxygen of the acetyl group in *O*AADPr is consistent with water addition to the proposed 1′,2′-cyclic intermediate formed after 2′-hydroxyl attack on the α-1′-*O*-alkylamidate. The effect of pH and of solvent viscosity on the k_{cat} values suggests that final product release is rate-limiting in the wild-type enzyme. Implications of this new evidence on the mechanisms of deacetylation and possible ADP-ribosylation catalyzed by Sir2 deacetylases are discussed.

The growing interest in the silent information regulator 2 (Sir2[1] or sirtuin) family of proteins lies in their involvement in a rapidly expanding list of cellular processes including gene silencing (*1*, *2*), cell cycle regulation (*3*), fatty acid metabolism (*4*), apoptosis (*5*−*7*), and life-span extension (*8*−*10*). Conserved among all forms of life with five homologues in yeast (ySir2 and HST1−4) and seven in humans (SIRT1−7) (*11*, *12*), most sirtuins display NAD^+-dependent protein deacetylase activity (*13*−*16*). SIRT1 has received the most attention and is reported to deacetylate a growing number of substrates including PGC-1α (*17*, *18*), FOXO proteins (*19*−*21*), and HIV Tat protein (*22*), suggesting its involvement in a broad range of biological processes such as glucose homeostasis, cell survival under stress, and HIV transcription. In contrast to the primarily nuclear SIRT1, SIRT2 is localized to the cytoplasm where it can deacetylate α-tubulin (*23*), and SIRT3, SIRT4, and SIRT5 are located in the mitochondrial matrix (*24*−*26*), but knowledge of their cellular targets is uncertain. The other human homologues, SIRT6 and SIRT7, are found in the nucleus (*24*), where SIRT6 is reported to possess ADP-ribosyltransferase activity (*27*).

The majority of Sir2 homologues are protein deacetylases catalyzing the conversion of NAD^+ and an acetylated lysine residue to nicotinamide, the corresponding deacetylated lysine residue, and 2′-*O*-acetyl-ADP-ribose (*O*AADPr) (Scheme 1) (*28*−*30*). This mechanism differs from that of class I and II histone deacetylases (HDACs), in which an active site zinc directs hydrolysis of the acetylated lysine residues to acetate and free lysine (*31*). This unusual consumption of NAD^+ in sirtuins (class III HDACs) with linked generation of the novel product *O*AADPr has led to the idea that *O*AADPr possesses unique biological properties whose cellular levels may be tightly regulated (*32*). Indeed, *O*AADPr was shown to be metabolized by a variety of cell extracts (*33*, *34*). In more recent evidence, *O*AADPr was shown to bind specifically to the histone splice variant macro H2A1.1 (*35*) and to induce formation of the yeast Sir2/Sir3/Sir4 complex in vitro (*36*).

The growing list of reported Sir2 substrates and the generation of the potential secondary messenger, *O*AADPr, has led to increased efforts to elucidate the molecular basis of Sir2-catalyzed deacetylation. Previously, kinetic analyses have shown that Sir2 deacetylases follow a sequential

† This work was supported by National Institutes of Health Grant GM065386 (to J.M.D.) and by National Institutes of Health Biotechnology Training Grant NIH 5 T32 GM08349 (to B.C.S.). This study was also supported by National Science Foundation Grant NSF CHE-9629688 for the NMR spectrometer used.

* To whom correspondence should be addressed. Tel: (608) 265-1859. Fax: (608) 262-5253. E-mail: jmdenu@wisc.edu.

‡ Department of Chemistry, University of Wisconsin—Madison.

§ Department of Biomolecular Chemistry, University of Wisconsin—Madison.

[1] Abbreviations: Sir2, silent information regulator 2; NAD^+, nicotinamide adenine dinucleotide, oxidized form; ADPr, adenosine 5′-diphosphoribose; *O*AADPr, *O*-acetyl-ADP-ribose.

10.1021/bi052014t CCC: $33.50 © 2006 American Chemical Society
Published on Web 12/07/2005

Scheme 1: General Reaction Catalyzed by Sir2 Protein Deacetylases

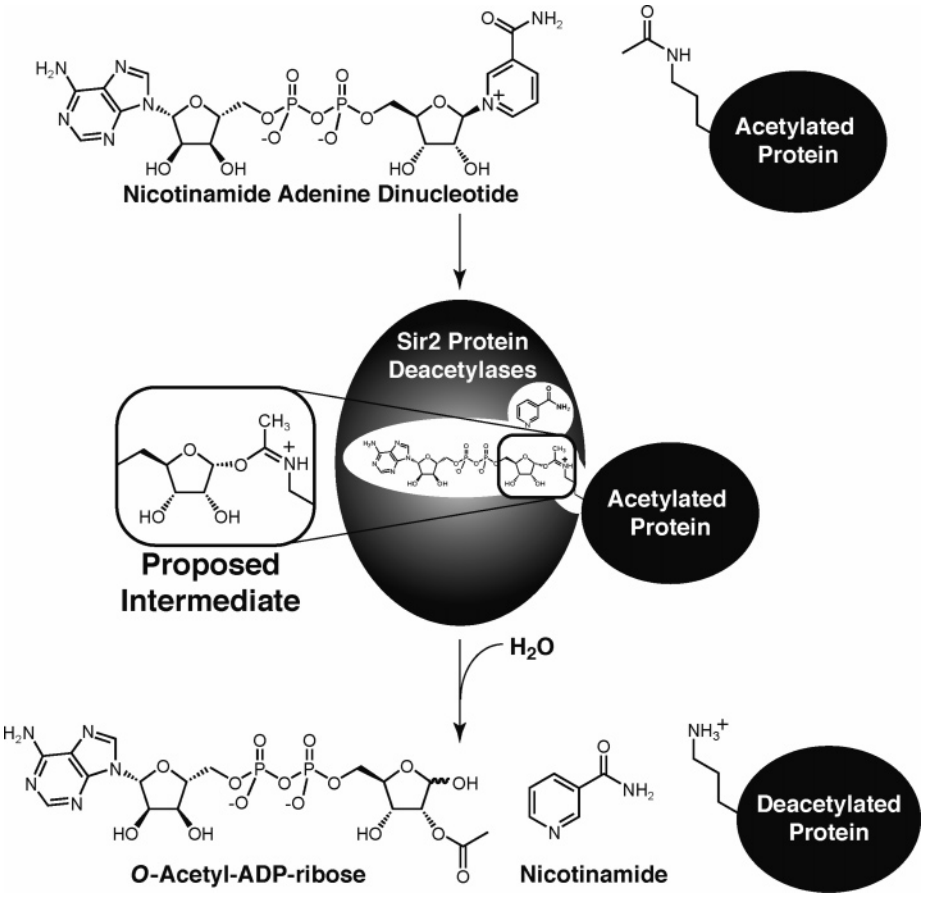

mechanism in which acetylated protein and then NAD^+ bind to form a ternary complex before chemical catalysis occurs in two kinetically distinct steps (*37*). In the initial chemical step, nicotinamide is released upon formation of an enzyme−ADP-ribose−acetylated protein intermediate, which has been postulated to be an α-1′-*O*-alkylamidate (Scheme 1) (*28*−*30*). One line of evidence for an α-1′-*O*-alkylamidate is the ability of nicotinamide, a potent product inhibitor (*15*, *16*, *38*−*40*), to rapidly react with the enzyme−ADP-ribose−acetylated protein intermediate, regenerating NAD^+ and acetylated protein by a process dubbed the nicotinamide exchange (or transglycosidation) reaction (*39*, *40*). In addition, the 2′-hydroxyl of NAD^+ does not play a significant role in the first chemical step since replacement with fluorine results in only a slight decrease in the nicotinamide exchange rate (*39*). This suggested that the initial step occurs exclusively about the 1′-position and that the acetylated lysine carbonyl oxygen acts as a nucleophile directly displacing nicotinamide. However, little evidence has been presented to support this hypothesis. In the second chemical step, the acetyl group is transferred to the ADP-ribose portion of NAD^+. It is believed that an active site histidine acts as the general base, activating the 2′-hydroxyl for acetyl transfer, but direct evidence for this is also lacking.

Here, we report direct evidence supporting the nucleophilic attack of the acetyllysine oxygen at the α face of the nicotinamide ribose to form a covalent α-1′-*O*-alkylamidate intermediate. In addition, we provide biochemical evidence for the role of the active site histidine as a general base and for the identity of the rate-limiting step in Sir2 catalysis. The implications of these findings on both the mechanism of deacetylation and the potential mechanism of ADP-ribosylation are discussed.

EXPERIMENTAL PROCEDURES

Materials and Methods. Synthetic 11-mer H3 peptide and acetylated H3 peptide (AcH3), corresponding to the 11 amino acids surrounding and including lysine-14 of the histone H3 N-terminal tail, H_2N-KSTGGK(Ac)APRKQ-$CONH_2$, were purchased from the University of Wisconsin−Madison peptide synthesis center, ^{3}H-labeled acetyl H3 peptide (^{3}H-AcH3) was synthesized enzymatically from the 11-mer H3 peptide as previously reported (*33*). ^{18}O-Labeled water was purchased from Cambridge Isotope Laboratories, Inc. (Andover, MA). All other chemicals used were of the highest purity commercially available and were purchased from Sigma (St. Louis, MO), Aldrich (Milwaukee, WI), or Fisher Scientific (Pittsburgh, PA). All mass spectral analyses were performed at the University of Wisconsin−Madison Biotechnology Center mass spectrometry facility.

Expression and Purification of His-Tagged HST2 WT and HST2 H135A. The expression and purification of histidine-tagged full-length HST2 WT and HST2 H135A were performed as previously reported (*30*, *39*), and the concentration of enzyme was determined using the method of Bradford (*41*). Enzyme aliquots were stored at −20 °C until ready for use.

Synthesis of ^{18}O-AcH3. Synthetic ^{18}O-labeled acetylated H3 peptide (^{18}O-AcH3), H_2N-KSTGGK(^{18}O-Ac)APRKQ-$CONH_2$, was synthesized using standard tBu/Fmoc solid-phase peptide synthesis techniques and HBTU/HOBt cou-

pling conditions (*42*). The ^{18}O label was specifically incorporated at the desired lysine side chain by using an ivDde protecting group that was orthogonally deprotected with 2% hydrazine in DMF. The liberated ϵ-amino group was then coupled to ^{18}O-labeled acetic acid using HBTU/HOBt coupling conditions, resulting in the full-length peptide, which was then deprotected and cleaved from the resin using TFA.

^{18}O-Labeling Experiments. Experiments for HST2 WT were done in 60 μL reaction volumes containing 1 mM DTT, 200 μM ^{18}O-AcH3, 185 μM NAD^+, 10 μM HST2, in natural abundance water or 90% $^{18}OH_2$ (98% ^{18}O), and 20 mM pyridine buffer adjusted to pH 7 with formic acid and were reacted for 30 min at 25 °C. Reactions were split into three 20 μL aliquots and flash frozen in dry ice. One aliquot was submitted directly for mass spectral analysis [ESI, (−)-ion mode, Applied Biosystems, MDS Sciex API 365, LC/MS/MS triple quadrupole]. The other two aliquots were lyophilized and redissolved in 20 μL of 10% formic acid and 90% natural abundance OH_2 or $^{18}OH_2$ (98% ^{18}O) and incubated at room temperature for 2 h. These were then flash frozen and kept at −20 °C until ready for mass spectral analysis as above. The degree of ^{18}O incorporation was determined by examining the relative peak heights at *m*/*z* ∼600.5, ∼602.5, and ∼604.5 corresponding to incorporation of zero, one, or two ^{18}O atoms.

^{18}O-Labeling experiments for HST2 H135A were done in 80 μL reaction volumes containing 1 mM DTT, 400 μM AcH3 (11-mer), 500 μM NAD^+, 50 μM HST2 H135A, in natural abundance water or 84% $^{18}OH_2$ (98% ^{18}O), and 20 mM pyridine buffer adjusted to pH 7 with formic acid and were reacted for 30 min at 25 °C. Reactions were split into three aliquots and analyzed by ESI-MS as stated above for HST2 WT. The degree of ^{18}O incorporation was determined by examining the relative peak heights at *m*/*z* ∼558 and ∼560 for ADPr and *m*/*z* ∼600.5, ∼602.5, and ∼604.5 for *O*AADPr.

Measurement of the Rate of Nonenzymatic ^{18}O Incorporation of OAADPr. *O*AADPr was synthesized and purified as previously reported (*33*). Solutions of 16.5 μM *O*AADPr, 20 mM pyridine buffer adjusted to pH 7 with formic acid, and 90% $^{18}OH_2$ were made. Time points from 5 to 140 min were analyzed by ESI-MS without further processing. The fraction of ^{18}O incorporation was determined by the ratio of the peak height at *m*/*z* ∼602.5 corresponding to *O*AADPr with one ^{18}O label to the sum of the peak heights at *m*/*z* ∼600.5 and ∼602.5.

pH Profile Experiments. The effect of pH on the kinetic parameters of HST2 WT was determined over a pH range of 5.4−9.4. Reactions containing 150 μM ^3H-AcH3, 1 mM DTT, 0.02−2 μM HST2 WT, and varying concentrations of NAD^+ from 5 to 320 μM in TBA buffer (50 mM Tris-HCl, 50 mM BisTris-HCl, 100 mM sodium acetate) were analyzed by charcoal binding assay as published (*43*). To ensure initial rate conditions, the reactions were quenched before 10% of the substrate was converted to products. The effect of pH on HST2 H135A was determined over a pH range of 5.8−9.4 with 2−3 mM ^3H-AcH3, 1 mM DTT, 2−5 μM HST2 H135A, and varying concentrations of NAD^+ from 5 to 1280 μM in TBA buffer. Graphs of rate (s^{-1}) versus NAD^+ concentration were fitted to the Michaelis−Menten equation (eq 1) using Kaleidagraph (Synergy Software, Reading, PA) to obtain the kinetic parameters k_{cat} and k_{cat}/K_m. Plots of k_{cat} or k_{cat}/K_m versus pH were fitted to eq 2

$$v = k_{cat}S/(K_m + S) \quad (1)$$

$$v = C/(1 + H/K_a) \quad (2)$$

using KinetAsyst (IntelliKinetics, State College, PA), where C is the pH-independent value, K_a is the ionization constant, and H is the proton concentration.

Solvent Viscosity Studies. The effect of viscosity on HST2 WT and HST2 H135A was determined using sucrose as a microviscogen. The steady-state parameters for HST2 WT were determined using the charcoal binding assay (*43*) and 80 μL reaction volumes with 500 μM NAD^+, 2−64 μM ^3H-AcH3 (11-mer), 1 mM DTT, 0−34% w/v sucrose, and 30−40 nM HST2 WT in TBA buffer at pH 8. The steady-state parameters for HST2 H135A were determined using the charcoal binding assay (*43*) and 80 μL reaction volumes with 2 mM NAD^+, 150−2400 μM AcH3 (11-mer), 1 mM DTT, 0−34% w/v sucrose, and 2 μM HST2 H135A in TBA buffer at pH 8. Graphs of rate (s^{-1}) versus AcH3 concentration were fitted to eq 1 to obtain the kinetic parameters k_{cat} and k_{cat}/K_m in Kaleidagraph. The ratio of the k_{cat} measured at 0% sucrose (k_{cat}^0) to the k_{cat} at each concentration of sucrose was plotted versus the relative viscosity of each sucrose solution. The relative viscosities of the reaction solutions as a function of sucrose percentage were taken from those measured by Murray et al. (*44*).

Measurement of ADPr and OAADPr Formation with HST2 H135A. ADPr and *O*AADPr formation over time was measured using 20 μL reaction volumes with 400−600 μM AcH3 (11-mer), 1 mM DTT, 500−1000 μM ^{32}P-NAD^+, 20−200 μM HST2 H135A or 0.5−50 μM HST2 WT, and 20−50 mM Tris-HCl buffer at pH 7.5 at 25 °C. ADPr and *O*AADPr formation was measured using the previously described thin-layer chromatography (TLC) assay (*16*, *43*, *45*) with the following modifications. Reactions were quenched by spotting 1 μL time points of the reactions directly onto the silica gel TLC plates. The plates were then run in 70:30 ethanol:2.5 M ammonium acetate and quantitated by phosphorimaging. Under these conditions *O*AADPr, ADPr, and NAD^+ ran with an average R_f of 0.53, 0.42, and 0.26, respectively.

Trapping of an Enzyme−ADPr−Acetyllysine Intermediate in HST2 H135A with MeOH and EtOH. Twenty microliter reaction volumes containing 1 mM DTT, 400 μM AcH3 (11-mer), 500 μM NAD^+, 50 μM HST2 H135A, 20% alcohol by volume (4.93 M MeOH or 3.39 M EtOH), and 20 mM pyridine buffer adjusted to pH 7 with formic acid were reacted for 30 min at 25 °C. Reactions were flash frozen in dry ice and stored at −20 °C until ready for ESI-MS analysis as outlined above for the ^{18}O-labeling experiments. A control reaction was run with the above conditions and 21 μM HST2 WT to determine if the methanolysis observed was specific to the mutant enzyme. A no-enzyme control was run with 500 μM ADPr replacing NAD^+ and the above conditions to measure the nonenzymatic methanol incorporation over 30 min.

Synthesis, Purification, and Characterization of 1′-O-Methyl-ADPr. A 1 mL reaction containing 1.8 mM AcH3 (11-mer), 2 mM NAD^+, 1 mM DTT, 100 μM HST2 H135A,

5 M methanol, and 50 mM Tris-HCl pH 7.5, was reacted for 2.5 h at 25 °C and quenched with TFA to a final concentration of 1%. The 1′-*O*-methyl-ADPr formed during this reaction was purified on a reversed-phase, small-pore C_{18} column (Vydac, Hesperia, CA) eluting with 0−20% acetonitrile (with 0.02% TFA) in water (with 0.05% TFA) and further purified on a poly(hydroxyethyl)aspartamide column (The Nest Group, Inc., Southboro, MA) eluting with 30 mM ammonium acetate and a gradient of 15−100% water in acetonitrile. Fractions containing the purified product were pooled and lyophilized twice from D_2O and then dissolved in 50 mM potassium phosphate buffer, pD 7.1. ^{1}H NMR spectra were obtained at 500 MHz on a Varian INOVA-500 NMR spectrometer and compared to previously published spectra for stereochemical assignment (*46*).

Measurement of the Relative Formation of ADPr and 1′-O-Methyl-ADPr by HST2 H135A. Reactions of 60 or 120 μL containing 0.5−4 M methanol, 400 μM AcH3 (11-mer), 500 μM ^{32}P-NAD$^+$, 1 mM DTT, 50 μM HST2 H135A, and 50 mM Tris-HCl buffer at pH 7.5 were reacted at 25 °C for 30 min. The reactions were analyzed by the previously described HPLC assay (*43*) and quantitated by UV absorbance of the adenine base at 260 nm or scintillation counting of the collected fractions. The product partitioning ratio, *K*, at each concentration of methanol was calculated from eq 3 assuming a water concentration of 55 M.

$$K = ([1'\text{-}O\text{-methyl-ADPr}][H_2O])/([\text{ADPr}][\text{MeOH}]) \quad (3)$$

RESULTS AND DISCUSSION

Source of New Oxygens in the Product OAADPr. The Sir2 reaction incorporates two new oxygens into the product, *O*AADPr, one from the net hydrolysis of the glycosidic bond and one from acetyl group transfer to *O*AADPr. The source of these oxygens presumably is from water and the acetyl oxygen of the acetylated lysine residue. Therefore, determining the precise fate (i.e., location about the ribose ring) of these oxygens as they are transferred to *O*AADPr is essential in support of the proposed α-1′-*O*-alkylamidate intermediate (Scheme 1). This was accomplished through specific ^{18}O-labeling experiments followed by mass spectral analysis.

The yeast Sir2 homologue, HST2, was reacted with NAD$^+$ and an 11-mer peptide based on the N-terminal tail of histone H3 [H_2N-KSTGGK(^{18}O-Ac)APRK-CONH$_2$, ^{18}O-AcH3] with a specific ^{18}O label at the side chain corresponding to acetylated lysine-14. This reaction revealed the incorporation of one ^{18}O label into *O*AADPr as seen by the major ESI-MS peak at *m*/*z* 602.4 (Figure 1A). Control experiments confirmed that this incorporation was enzymatic, instead of nonenzymatic incorporation over time (Figure 1B). Incubation of a lyophilized aliquot of the original reaction solution in 10% formic acid with [^{18}O]water resulted in no change in mass (Figure 1A). However, the transferred ^{18}O label was completely washed out when a separate lyophilized aliquot was redissolved in 10% formic acid in natural abundance water, as shown by the major ESI-MS peak at *m*/*z* 600.5 (Figure 1A). This indicated that the ^{18}O label from ^{18}O-AcH3 was specifically transferred to the 1′-hydroxyl of *O*AADPr since only the 1′-hydroxyl can exchange with bulk solvent under these acidified conditions. This result presents the first direct evidence for the attack of the acetylated lysine oxygen at the 1′-position of the nicotinamide ribose to form the initial α-1′-*O*-alkylamidate intermediate.

Reactions of HST2 were then carried out with ^{18}O-AcH3 peptide and [^{18}O]water, resulting in the major mass spectral peak at *m*/*z* 604.4, indicating incorporation of ^{18}O labels at two separate positions (Figure 1A). Incorporation of two labels confirmed that water was the source of the other new oxygen in *O*AADPr. Subsequent acid exchange of *O*AADPr in natural abundance water showed a decrease of two mass units as seen by a peak at 602.4 *m*/*z*, indicating the label arising from water was in a nonexchangeable position (Figure 1A). The fact that the ^{18}O label from water could not be exchanged indicated its placement as the acetyl carbonyl oxygen in *O*AADPr, consistent with a previous report by Sauve and Schramm (*29*).

Effect of pH on the Activity of HST2 WT and HST2 H135A. The active site histidine corresponding to His-135 in HST2 is invariant among Sir2 enzymes. From the known crystal structures with either NAD$^+$, ADPr, or *O*AADPr bound (*47*−*52*), the side chain imidazole group of this histidine is generally positioned near the 3′-hydroxyl of the NAD$^+$ nicotinamide ribose. This histidine has therefore been postulated to be the general base responsible for activating the 2′-hydroxyl for attack of the proposed α-1′-*O*-alkylamidate intermediate and subsequent acetyl transfer to the 2′-position.

To provide direct biochemical evidence for His-135 as a general base in the Sir2 deacetylation mechanism, the effect of pH on the k_{cat}/K_m and k_{cat} of both HST2 and the corresponding histidine-to-alanine mutant enzyme, HST2 H135A, was determined. These experiments were performed by varying NAD$^+$ at saturating AcH3 concentrations such that the pH dependency of k_{cat}/K_m would reflect ionizations critical for any steps from NAD$^+$ binding to nicotinamide release. Determination of HST2 WT k_{cat}/K_m values over a pH range from 5.4 to 9.4 revealed a critical ionization with a pK_a value of 6.77 ± 0.06 that must be unprotonated for activity (Figure 2A), consistent with the pK_a expected for a histidine side chain. Conversely, the k_{cat}/K_m profile for HST2 H135A exhibited no pH dependence over the range tested, with k_{cat}/K_m values 2 orders of magnitude lower than wild type at high pH [(2.75 ± 0.22) × 10^4 M^{-1} s^{-1} for HST2 WT versus (1.5 ± 0.2) × 10^2 M^{-1} s^{-1} for HST2 H135A]. It was previously shown that HST2 H135A exhibits only a 3-fold lower nicotinamide exchange rate compared to HST2 WT, suggesting that His-135 does not participate significantly in the chemical steps involving nicotinamide cleavage and release (*39*). Therefore, the critical ionization seen in the wild-type k_{cat}/K_m pH profile is consistent with the His-135 side chain binding and positioning NAD$^+$ into its catalytically productive conformation.

Conversely, the k_{cat} pH profile for HST2 WT showed no critical ionizations but did show a slight pH dependence that varied only 3−4-fold (0.07 s^{-1} at low pH and 0.26 s^{-1} at high pH) across >4 pH units (Figure 2B). The lack of a critical ionization is consistent with a pH-independent product release step limiting turnover, as was previously suggested (*37*). In contrast, HST2 H135A exhibited k_{cat} values 1−2 orders of magnitude lower than wild-type enzyme (0.26 ± 0.03 vs 0.026 ± 0.005 s^{-1} at high pH) and a pH dependency on k_{cat} revealing an ionization (pK_a 7.43 ± 0.13) that must be unprotonated for activity (Figure 2B). This decrease in

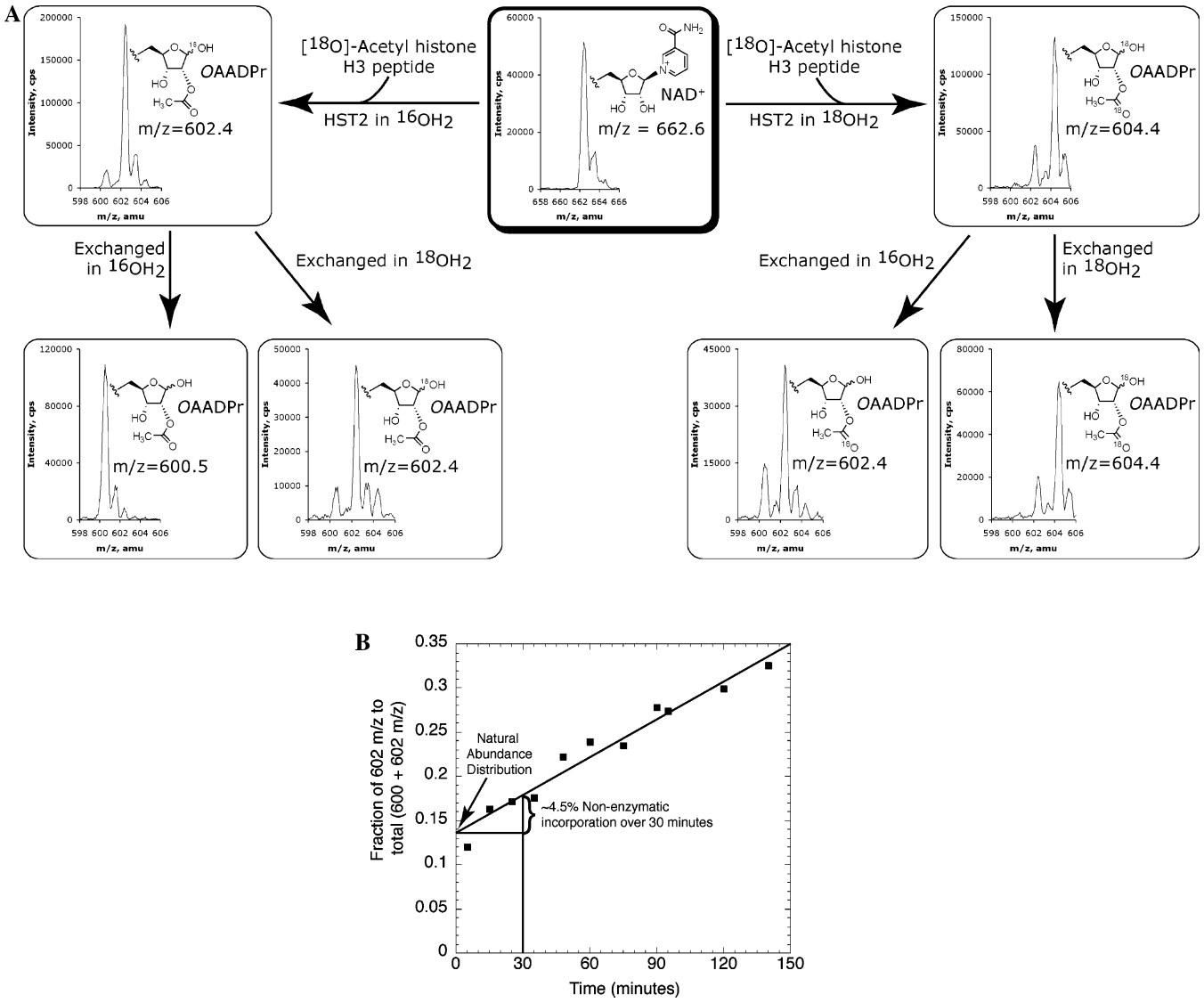

FIGURE 1: (A) ^{18}O-labeling experiments with HST2 WT. Reactions contained 1 mM DTT, 200 μM ^{18}O-AcH3, 185 μM NAD$^+$, 10 μM HST2, in natural abundance water or 90% $^{18}OH_2$, and 20 mM pyridine buffer at pH 7. Each reaction was split into three aliquots, two of which were lyophilized and exchanged in 10% formic acid and 90% natural abundance OH_2 or $^{18}OH_2$. ^{18}O incorporation was determined by examining the relative peak heights at *m*/*z* ~600.5, ~602.5, and ~604.5 corresponding to zero, one, or two ^{18}O atoms. (B) Rate of nonenzymatic exchange of an ^{18}O label from water into *O*AADPr. Purified *O*AADPr was diluted to 16.5 μM in 20 mM pyridine buffer and 90% $^{18}OH_2$ at pH 7. Time points were injected directly into the mass spectrometer. The *y*-intercept, which represents the zero time point before exposing *O*AADPr to [^{18}O]water, was calculated as 13.3% and is consistent with the natural distribution of heavy isotopes across the entire *O*AADPr molecule. A rate of nonenzymatic incorporation of 0.15%/min was calculated, which corresponds to a maximum of 4.5% nonenzymatic incorporation for the 30 min reaction time used in our assays.

reaction rate (10-fold at pH values >8), coupled with the alteration in the pH dependency, indicates a change in the rate-limiting step from a pH-independent step (observed with wild type) to a pH-dependent chemical step in HST2 H135A. The source of the ionization observed in the mutant k_{cat} pH profile is unclear. It would be attractive to suggest that this group, which must be unprotonated, is the ribose 2′-OH; however, with an apparent pK_a of 7.4, this would be ~5 pH units lower than that expected, making this possibility seem implausible. On the other hand, the flattening out of the curve above an apparent pK_a of 7.4 may result from a downstream pH-independent step beginning to limit turnover at very high pH, whereas at low pH, the rate increases as a function of the 2′-OH ionization.

As mentioned earlier, the Sir2 chemical reaction can be kinetically resolved into two main steps: (1) attack of the acetyllysine oxygen to form the proposed α-1′-*O*-alkylamidate with nicotinamide release and (2) attack of the 2′-hydroxyl at the proposed α-1′-*O*-alkylamidate and subsequent acetyl transfer to form *O*AADPr (*28*−*30*, *37*, *39*, *40*). The small 3-fold change in the nicotinamide exchange rate observed between HST2 WT and HST2 H135A (*39*) suggests that the slowed catalytic step seen in the HST2 H135A k_{cat} pH profile (Figure 2B) occurs after nicotinamide cleavage and release but before *O*AADPr and peptide release. By default, this affected step would be the 2′-hydroxyl attack of the α-1′-*O*-alkylamidate intermediate, which is expedited in wild type by His-135 functioning as the general base but is impaired in HST2 H135A. This possibility was explored further in subsequent experiments.

Effect of Viscosity on the Rate of Deacetylation. The lack of pH dependency on the k_{cat} for the wild-type enzyme suggested that product release might be rate-limiting. To test this hypothesis, solvent viscosity studies were carried out.

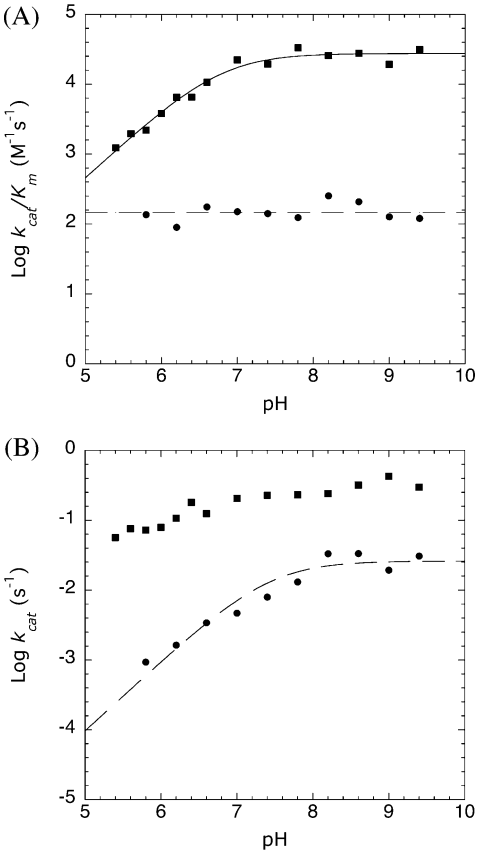

FIGURE 2: pH rate profiles. Reaction rates were determined on the basis of *O*AADPr formation. Reactions for HST2 WT contained 150 μM ^{3}H-AcH3, 1 mM DTT, 0.02−2 μM HST2 WT, and varying concentrations of NAD^+ from 5 to 320 μM in TBA buffer. The reaction for HST2 H135A contained 2−3 mM ^{3}H-AcH3, 1 mM DTT, 2−5 μM HST2 H135A, and varying concentrations of NAD^+ from 5 to 1280 μM in TBA buffer. (A) Effect of pH on k_{cat}/K_m varying NAD^+ for HST2 WT (squares) and HST2 H135A (circles). HST2 WT displayed a critical ionization with a pK_a of 6.77 ± 0.06, while HST2 H135A exhibited no effect over the pH range tested. (B) Effect of pH on k_{cat} for HST2 WT (squares) and HST2 H135A (circles). HST2 H135A displayed a critical ionization with a pK_a of 7.43 ± 0.13 while HST2 WT showed no critical ionizations over the pH range tested.

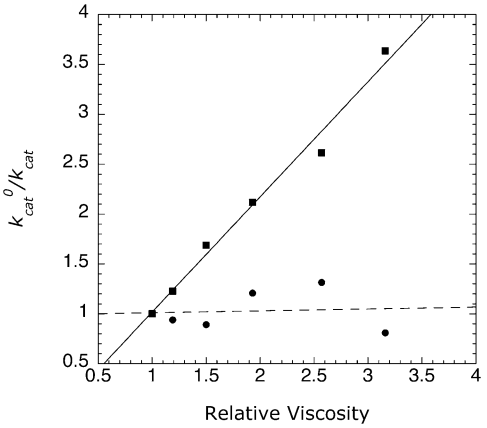

FIGURE 3: Effect of viscosity on k_{cat}. Reaction rates were determined on the basis of *O*AADPr formation. k_{cat}^0/k_{cat} is the k_{cat} in the absence of sucrose divided by the k_{cat} measured at each concentration of sucrose. HST2 WT (squares) reactions contained 500 μM NAD^+, 2−64 μM AcH3 (11-mer form), 1 mM DTT, 0−34% w/v sucrose, and 2 μM HST2 H135A in TBA buffer at pH 8. HST2 H135A (circles) reactions contained 2 mM NAD^+, 150−2400 μM AcH3 (11-mer), 1 mM DTT, 0−34% w/v sucrose, and 30−40 nM HST2 WT in TBA buffer at pH 8. Linear regression analysis showed a slope of 1.15 ± 0.07 for HST2 WT and 0.02 ± 0.12 for HST2 H135A.

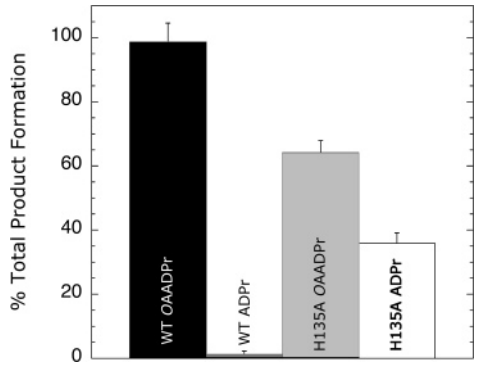

FIGURE 4: Relative formation of ADPr and *O*AADPr. Reactions contained 400−600 μM AcH3 (11-mer), 1 mM DTT, 500−1000 μM ^{32}P-NAD^+, 20−200 μM HST2 H135A or 0.5−50 μM HST2 WT, and 20−50 mM Tris-HCl buffer at pH 7.5 and 25 °C. The ADPr observed from HST2 WT was at background levels, and its formation did not increase over time. Each column was normalized to the total product formed a each time point. Error bars represent standard deviations.

Since the diffusion rate of small molecules is inversely proportional to the viscosity of the solvent (*53*), the overall rate of enzymatic reactions in which product release or substrate association is rate-limiting can display a linear dependence on the viscosity of the solution (*54*−*57*). In the case of product release, this step could be either the dissociation of product from the enzyme or a conformational change allowing dissociation. Therefore, a slope equal to unity in a plot of the inverse of the relative rate constant (k_{cat}^0/k_{cat}) versus the relative viscosity of the solution reflects a substrate association or product release as rate-limiting step, whereas a slope of zero reflects a non-diffusion-mediated step such as chemical catalysis. Indeed, using sucrose as a viscogen, we found that the k_{cat} of HST2 WT varied linearly (slope = 1.15 ± 0.07) with the relative viscosity of the solution (Figure 3). In contrast, the k_{cat} of HST2 H135A displayed no dependence on viscosity (Figure 3). The k_{cat}/K_m values with acetylated peptide also displayed no viscosity dependence (data not shown). With an overall turnover rate of ~0.26 s^{-1} for HST2 WT, the viscosity dependence observed is likely due to a conformational change within the active site allowing product (*O*AADPr and/or peptide) release, whereas the mutant enzyme rate appears to be restricted at the chemical step involving 2′-hydroxyl attack of the α-1′-*O*-alkylamidate intermediate.

Partitioning between ADPr and OAADPr in HST2 H135A. While analyzing the H135A mutant enzyme, we observed significant production of ADP-ribose (ADPr) during turnover that also yielded *O*AADPr (*39*). As *O*AADPr is susceptible to nonenzymatic hydrolysis to form ADPr and acetate, it was important to establish the source of observed ADPr. The relative amounts of ADPr and *O*AADPr formed in the enzyme reactions were measured as outlined under Experimental Procedures. From these assays, it was confirmed that ADPr formation observed with HST2 H135A was not from hydrolysis of *O*AADPr but was due to inherent activity of HST2 H135A (Figure 4). The negligible ADPr detected for HST2 WT did not exceed background levels and did not increase over time (Figure 4). In addition, HST2 H135A

Scheme 2: Proposed Mechanism of Formation of both ADPr and *O*AADPr

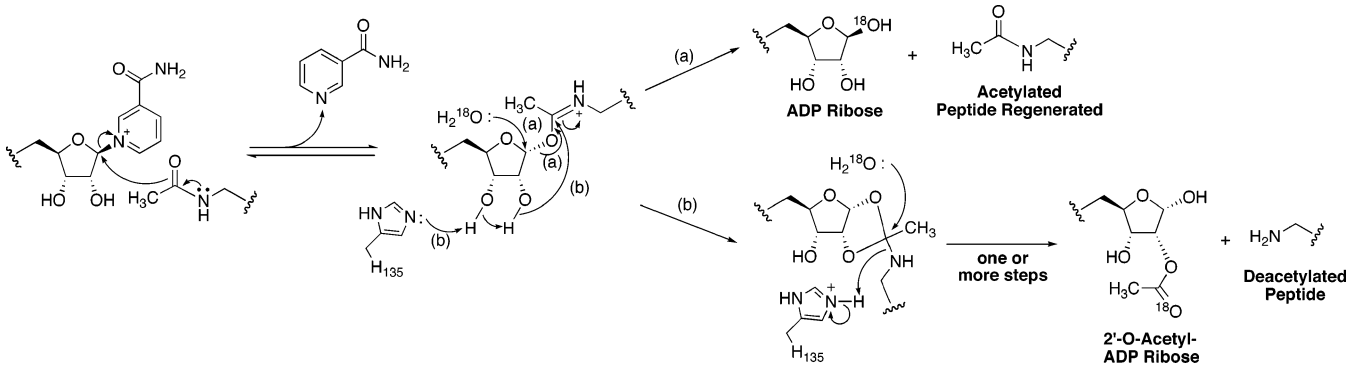

formed products *O*AADPr:ADPr in a constant ratio of 25:14 over the entire time course of this assay, suggesting partitioning of a common intermediate between attack of the 2′-hydroxyl to form *O*AADPr and hydrolysis to form ADPr (Scheme 2). With the H135A mutant, this partitioning is consistent with the lack of 2′-hydroxyl activation by His-135, resulting in the increased lifetime of the α-1′-*O*-alkylamidate intermediate such that hydrolysis to form ADPr now acts as a competing reaction with formation of *O*AADPr (pathway (a) in Scheme 2).

Hydrolysis of the Enzyme−ADPr−Acetyllysine Intermediate to ADP-ribose in HST2 H135A. To further characterize the mechanism by which HST2 H135A forms ADPr, ^{18}O-labeling experiments similar to those outlined above for HST2 WT were performed. Both ADPr and *O*AADPr showed the incorporation of a single ^{18}O label (Figure 5). Subsequent acid exchange of the 1′-hydroxyl in natural abundance water decreased the mass of ADPr by two mass units, indicating that the ^{18}O label from water was at the 1′-position in ADPr. The enzymatic formation of ADPr was completely dependent on the presence of the acetyllysine peptide, as control reactions lacking AcH3 showed no conversion of NAD^+ by ESI-MS (data not shown), indicating that the enzyme must be able to form the proposed α-1′-*O*-

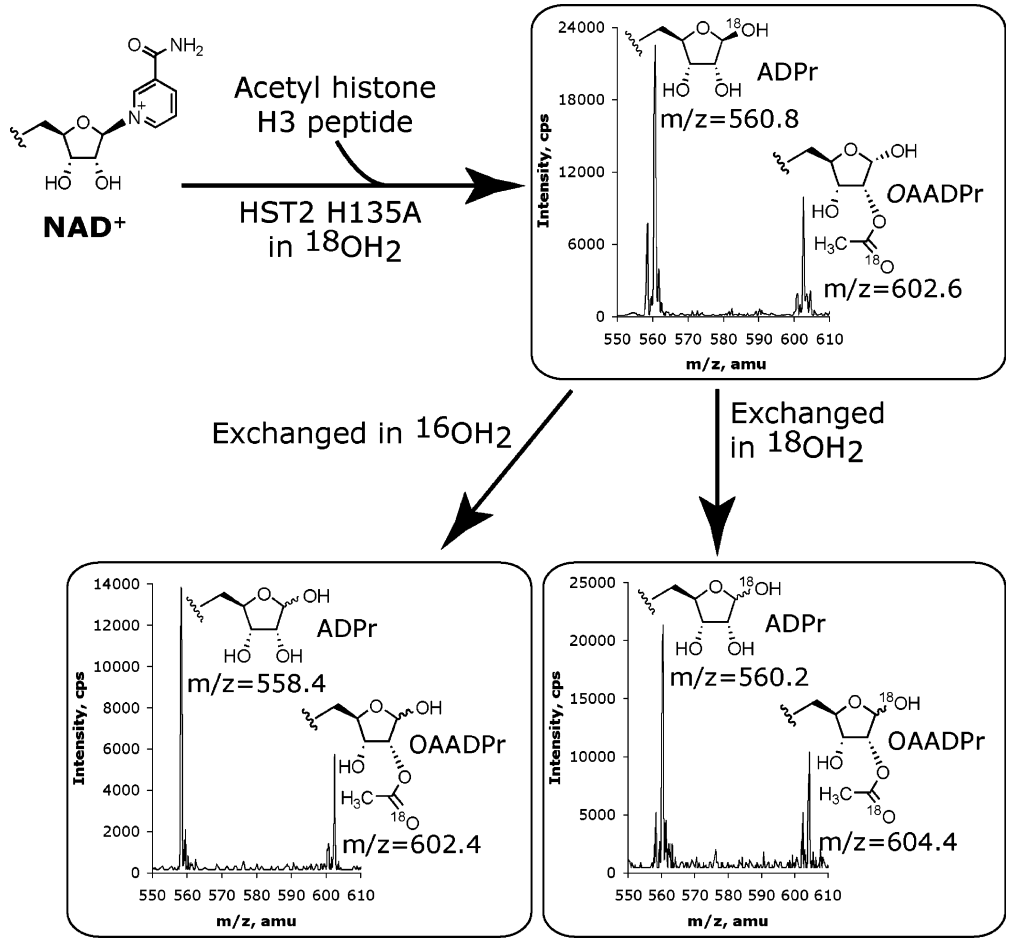

FIGURE 5: ^{18}O-Labeling experiments with HST2 H135A. Reactions contained 1 mM DTT, 400 μM AcH3 (11-mer), 500 μM NAD^+, 50 μM HST2 H135A, 84% $^{18}OH_2$, and 20 mM pyridine buffer adjusted at pH 7 and were reacted for 30 min at 25 °C. Reactions were split into three aliquots, two of which were lyophilized and then exchanged in 10% formic acid and 90% natural abundance OH_2 or $^{18}OH_2$. ^{18}O incorporation was determined by examining the relative peak heights at *m*/*z* ∼600.5, ∼602.5, and ∼604.5 corresponding to zero, one, or two ^{18}O atoms.

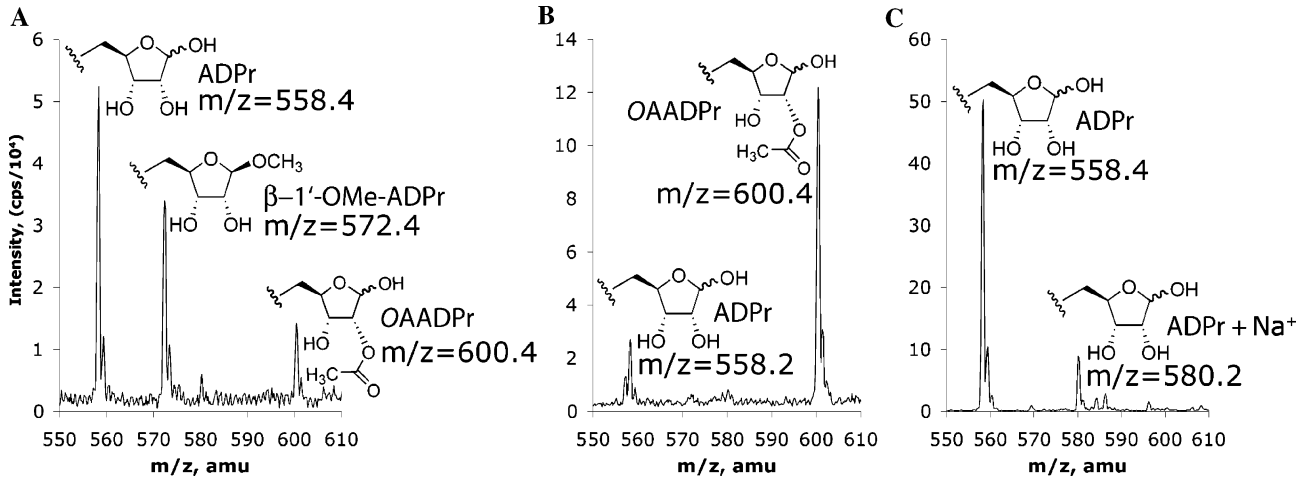

FIGURE 6: (A) ESI-MS of the 30 min reaction of HST2 H135A with 1 mM DTT, 400 μM AcH3 (11-mer), 500 μM NAD^+, 50 μM HST2 H135A, 20% v/v MeOH, and 20 mM pyridine buffer at pH 7 at 25 °C. HST2 H135A forms ADPr, 1′-*O*-methyl-ADPr, and *O*AADPr under these conditions. (B) ESI-MS of the 30 min control reaction of HST2 WT with 1 mM DTT, 400 μM AcH3 (11-mer), 500 μM NAD^+, 21 μM HST2 WT, 20% (v/v) MeOH, and 20 mM pyridine buffer at pH 7 at 25 °C. HST2 WT forms no detectable 1′-*O*-methyl-ADPr under these reaction conditions. (C) ESI-MS of the 30 min nonenzymatic incorporation of 20% (v/v) MeOH into 500 μM ADPr with 1 mM DTT, 400 μM AcH3 (11-mer), and 20 mM pyridine buffer at pH 7 at 25 °C. There was no detectable 1′-*O*-methyl-ADPr in this control. Therefore, the 1′-*O*-methyl-ADPr observed with HST2 H135A was due to enzymatic activity inherent in the mutant enzyme only.

alkylamidate intermediate in order for hydrolysis to ADPr to occur. Furthermore, AcH3 showed no incorporation of an ^{18}O label under the same reaction conditions by MALDI-MS (data not shown), adding to the evidence that hydrolysis to ADPr is due to the specific attack of water at the 1′-carbon of the nicotinamide ribose and not due to hydrolysis by attack of water at the imidate carbon of the α-1′-*O*-alkylamidate. In accordance with the previous ^{18}O-labeling experiments using HST2 WT, the ^{18}O label from *O*AADPr was non-exchangeable and, therefore, is located in the acetyl carbonyl oxygen, indicating that *O*AADPr is formed by the same mechanism in the mutant enzyme as in wild type. These HST2 H135A ^{18}O-labeling experiments are consistent with the proposed mechanism in which the hydrolysis to ADPr is in direct competition with the attack of the 2′-hydroxyl to form a 1′,2′-cyclic intermediate that is attacked by water to form *O*AADPr (Scheme 2).

Trapping of the Intermediate with Alcohol Nucleophiles. In the H135A mutant, the observed hydrolysis of the α-1′-*O*-alkylamidate to form ADPr suggested that exogenous alcohols could also be reacted. If so, this could provide additional evidence for the suggested stereochemistry and covalent nature of the α-1′-*O*-alkylamidate intermediate, since the 1′-*O*-alkyl-ADPr product formed from alcoholysis would be unable to undergo mutarotation. Therefore, H135A mutant reactions containing 20% methanol or ethanol by volume were reacted for 30 min and analyzed by ESI-MS. The spectra displayed a new product with a mass of *m*/*z* 572.4, consistent with 1′-*O*-methyl-ADPr for methanol-containing reactions, and a mass of *m*/*z* 586.4, consistent with 1′-*O*-ethyl-ADPr for ethanol-containing reactions (Figure 6A). Control reactions utilizing HST2 WT showed no formation of 1′-*O*-methyl-ADPr (Figure 6B). In addition, a no-enzyme control with ADPr, 20% methanol, and identical buffer conditions gave no detectable incorporation of methanol over 30 min (Figure 6C). Therefore, the formation of 1′-*O*-methyl-ADPr and 1′-*O*-ethyl-ADPr is specific to HST2 H135A and is the direct result of methanolysis or ethanolysis of an enzymatic intermediate.

To determine the stereochemistry of the enzyme-synthesized 1′-*O*-methyl-ADPr, this product was purified from the HST2 H135A reaction by reversed-phase and hydrophilic interaction HPLC and analyzed by NMR spectroscopy. The stereochemistry about the 1′-position was assigned as β by comparison with previously published spectra of β-1′-*O*-methyl-ADPr (*46*). Because Sir2 enzymes are not expected to possess an alcohol binding site that would direct alcohol attack stereoselectively, the stereochemical assignment of β-1′-*O*-methyl-ADPr provides direct evidence for a covalent intermediate formed on the α face of the ribose ring such that the alcohol nucleophiles react by a double-displacement mechanism. Together, these data strongly suggest the existence of a covalent α-1′-*O*-alkylamidate intermediate during Sir2 catalysis.

Methanolysis versus Hydrolysis Reactivity Profile. Previous studies of NAD^+ glycohydrolases have gained valuable insights into the reactivity of catalytic intermediates by measurement of the product-partitioning ratio, *K*, for methanolysis versus hydrolysis (*58*−*65*). Using 0.5−4 M methanol, we determined a product-partitioning ratio for HST2 H135A of 26.2 ± 3.3 compared to the range of values from 11 to 200 reported for other NAD^+ glycohydrolases (*58*−*65*). In contrast, nonenzymatic hydrolysis of NAD^+ shows no preference for methanol over water, as the product ratio simply reflects the molar ratio of methanol to water as well as the high reactivity of the oxocarbenium intermediate formed during solvolysis (*58*, *60*). Therefore, the selectivity for methanolysis observed here reflects enzyme stabilization of the intermediate compared to an oxocarbenium and indicates that the intermediate has significant bond order toward the incoming nucleophile. In addition, the ratio of methanolysis to hydrolysis was found to increase linearly with increasing concentrations of methanol, indicating that methanol was not saturating the active site and that the observed selectivity was due to the increased nucleophilicity of methanol toward the enzyme-stabilized α-1′-*O*-alkylamidate intermediate.

Implications toward the Mechanism of ADP-ribosylation As Catalyzed by Sir2 Homologues. Recently, several reports have suggested that some Sir2 homologues possess ADP-ribosyltransferase activity (*11*, *13*, *27*, *66*, *67*). These findings are still controversial as the ADP-ribosylation activity has not been demonstrated to be catalytic. The results presented here provide some additional insight into possible mechanisms of the observed ADP-ribosylation. In particular, the ability of HST2 H135A to react with exogenous alcohol nucleophiles suggests that the α-1′-*O*-alkylamidate intermediate may be able to accept other protein nucleophiles as well, as was recently hypothesized (*68*). Therefore, while the active site histidine corresponding to His-135 in HST2 is conserved across all yeast and human Sir2 homologues, this histidine may not be poised to activate the 2′-hydroxyl in Sir2 homologues that lack deacetylase activity. The loss of general-base activation of the 2′-hydroxyl could allow reaction of the stalled α-1′-*O*-alkylamidate with an incoming nucleophile resulting in ADP-ribosylation and regeneration of the acetylated residue. This nucleophile could be from either another protein, the acetylated protein that reacted to form the α-1′-*O*-alkylamidate, or the Sir2 protein itself (resulting in auto-ADP-ribosylation) (*68*). Although the above ADP-ribosylation mechanism requires an acetylated substrate to initiate formation of the α-1′-*O*-alkylamidate, it is possible that a Sir2 active site residue, such as an asparagine or glutamine, could replace the acetylated lysine residue to react in a manner similar to some NAD^+ modifying enzymes. For example, CD38 is suggested to go through a glutamate−ADP-ribose covalent intermediate at the 1′-position in its catalysis to form cyclic ADP-ribose (*69*). Future studies are necessary to reveal the significance of ADP-ribosylation activity from the sirtuin family of proteins.

CONCLUSION

In this study, we have presented valuable new insights into the chemical mechanism of Sir2 enzymes, using a variety of approaches including ^{18}O-labeling analysis, solvent perturbation, and mutant and wild-type pH rate analysis. We provided the first direct evidence for the attack of the acetylated lysine oxygen at the 1′-position of the nicotinamide ribose of NAD^+ to form an α-1′-*O*-alkylamidate intermediate. Measurement of the effect of pH on the k_{cat} and k_{cat}/K_m values for both HST2 WT and HST2 H135A supported the involvement of His-135 in both NAD^+ binding/positioning and activation of the 2′-hydroxyl for attack of the α-1′-*O*-alkylamidate intermediate. Lack of pH dependence on k_{cat} for HST2 WT suggested that product release was rate-limiting, a hypothesis supported through solvent viscosity experiments. The production of both *O*AADPr and ADPr by HST2 H135A was consistent with partitioning of the α-1′-*O*-alkylamidate intermediate between water attack and the 2′-hydroxyl of ribose. Hydrolysis required the presence of peptide substrate, and the intermediate exhibited a preference for methanolysis to give β-1′-*O*-methyl-ADPr.

Having established the existence of the α-1′-*O*-alkylamidate intermediate, future work will utilize these findings in the design of mechanism-based inhibitors and activators of Sir2 enzymes. The discovery of more potent and specific chemical regulators of Sir2 activity would permit more specific investigations of Sir2-dependent cellular pathways, as well as potential treatments of cancer, aging, diabetes, and neurodegeneration.

ACKNOWLEDGMENT

The authors thank members of the Denu group, especially Margie Borra and Chris Berndsen, for valuable discussions. We thank Norman Oppenheimer for helpful discussions and Michael Jackson for suggestions with the ^{18}O-labeling experiments. We also thank for Gary Case for peptide syntheses and Amy Harms for assistance with the mass spectrometry experiments.

REFERENCES

1. Rusche, L. N., Kirchmaier, A. L., and Rine, J. (2003) The establishment, inheritance, and function of silenced chromatin in *Saccharomyces cerevisiae*, *Annu. Rev. Biochem. 72*, 481−516.
2. Gasser, S. M., and Cockell, M. M. (2001) The molecular biology of the SIR proteins, *Gene 279*, 1−16.
3. Dryden, S. C., Nahhas, F. A., Nowak, J. E., Goustin, A. S., and Tainsky, M. A. (2003) Role for human SIRT2 NAD-dependent deacetylase activity in control of mitotic exit in the cell cycle, *Mol. Cell. Biol. 23*, 3173−3185.
4. Starai, V. J., Celic, I., Cole, R. N., Boeke, J. D., and Escalante-Semerena, J. C. (2002) Sir2-dependent activation of acetyl-CoA synthetase by deacetylation of active lysine, *Science 298*, 2390−2392.
5. Vaziri, H., Dessain, S. K., Ng Eaton, E., Imai, S. I., Frye, R. A., Pandita, T. K., Guarente, L., and Weinberg, R. A. (2001) hSIR2-(SIRT1) functions as an NAD-dependent p53 deacetylase, *Cell 107*, 149−159.
6. Luo, J., Nikolaev, A. Y., Imai, S., Chen, D., Su, F., Shiloh, A., Guarente, L., and Gu, W. (2001) Negative control of p53 by Sir2alpha promotes cell survival under stress, *Cell 107*, 137−148.
7. Langley, E., Pearson, M., Faretta, M., Bauer, U. M., Frye, R. A., Minucci, S., Pelicci, P. G., and Kouzarides, T. (2002) Human SIR2 deacetylates p53 and antagonizes PML/p53-induced cellular senescence, *EMBO J. 21*, 2383−2396.
8. Kaeberlein, M., McVey, M., and Guarente, L. (1999) The SIR2/3/4 complex and SIR2 alone promote longevity in *Saccharomyces cerevisiae* by two different mechanisms, *Genes Dev. 13*, 2570−2580.
9. Rogina, B., and Helfand, S. L. (2004) Sir2 mediates longevity in the fly through a pathway related to calorie restriction, *Proc. Natl. Acad. Sci. U.S.A. 101*, 15998−16003.
10. Tissenbaum, H. A., and Guarente, L. (2001) Increased dosage of a sir-2 gene extends lifespan in *Caenorhabditis elegans*, *Nature 410*, 227−230.
11. Frye, R. A. (1999) Characterization of five human cDNAs with homology to the yeast SIR2 gene: Sir2-like proteins (sirtuins) metabolize NAD and may have protein ADP-ribosyltransferase activity, *Biochem. Biophys. Res. Commun. 260*, 273−279.
12. Frye, R. A. (2000) Phylogenetic classification of prokaryotic and eukaryotic Sir2-like proteins, *Biochem. Biophys. Res. Commun. 273*, 793−798.
13. Imai, S., Armstrong, C. M., Kaeberlein, M., and Guarente, L. (2000) Transcriptional silencing and longevity protein Sir2 is an NAD-dependent histone deacetylase, *Nature 403*, 795−800.
14. Smith, J. S., Brachmann, C. B., Celic, I., Kenna, M. A., Muhammad, S., Starai, V. J., Avalos, J. L., Escalante-Semerena, J. C., Grubmeyer, C., Wolberger, C., and Boeke, J. D. (2000) A phylogenetically conserved NAD^+-dependent protein deacetylase activity in the Sir2 protein family, *Proc. Natl. Acad. Sci. U.S.A. 97*, 6658−6663.
15. Landry, J., Slama, J. T., and Sternglanz, R. (2000) Role of NAD-(+) in the deacetylase activity of the SIR2-like proteins, *Biochem. Biophys. Res. Commun. 278*, 685−690.
16. Landry, J., Sutton, A., Tafrov, S. T., Heller, R. C., Stebbins, J., Pillus, L., and Sternglanz, R. (2000) The silencing protein SIR2 and its homologs are NAD-dependent protein deacetylases, *Proc. Natl. Acad. Sci. U.S.A. 97*, 5807−5811.
17. Rodgers, J. T., Lerin, C., Haas, W., Gygi, S. P., Spiegelman, B. M., and Puigserver, P. (2005) Nutrient control of glucose

homeostasis through a complex of PGC-1alpha and SIRT1, *Nature 434*, 113−118.
18. Nemoto, S., Fergusson, M. M., and Finkel, T. (2005) SIRT1 functionally interacts with the metabolic regulator and transcriptional coactivator PGC-1{alpha}, *J. Biol. Chem. 280*, 16456−16460.
19. Brunet, A., Sweeney, L. B., Sturgill, J. F., Chua, K. F., Greer, P. L., Lin, Y., Tran, H., Ross, S. E., Mostoslavsky, R., Cohen, H. Y., Hu, L. S., Cheng, H. L., Jedrychowski, M. P., Gygi, S. P., Sinclair, D. A., Alt, F. W., and Greenberg, M. E. (2004) Stress-dependent regulation of FOXO transcription factors by the SIRT1 deacetylase, *Science 303*, 2011−2015.
20. Motta, M. C., Divecha, N., Lemieux, M., Kamel, C., Chen, D., Gu, W., Bultsma, Y., McBurney, M., and Guarente, L. (2004) Mammalian SIRT1 represses forkhead transcription factors, *Cell 116*, 551−563.
21. Daitoku, H., Hatta, M., Matsuzaki, H., Aratani, S., Ohshima, T., Miyagishi, M., Nakajima, T., and Fukamizu, A. (2004) Silent information regulator 2 potentiates Foxo1-mediated transcription through its deacetylase activity, *Proc. Natl. Acad. Sci. U.S.A. 101*, 10042−10047.
22. Pagans, S., Pedal, A., North, B. J., Kaehlcke, K., Marshall, B. L., Dorr, A., Hetzer-Egger, C., Henklein, P., Frye, R., McBurney, M. W., Hruby, H., Jung, M., Verdin, E., and Ott, M. (2005) SIRT1 regulates HIV transcription via Tat deacetylation, *PLoS Biol. 3*, e41.
23. North, B. J., Marshall, B. L., Borra, M. T., Denu, J. M., and Verdin, E. (2003) The human Sir2 ortholog, SIRT2, is an NAD^+-dependent tubulin deacetylase, *Mol. Cell 11*, 437−444.
24. Michishita, E., Park, J. Y., Burneskis, J. M., Barrett, J. C., and Horikawa, I. (2005) Evolutionarily conserved and nonconserved cellular localizations and functions of human SIRT proteins, *Mol. Biol. Cell 16*, 4623−4635.
25. Onyango, P., Celic, I., McCaffery, J. M., Boeke, J. D., and Feinberg, A. P. (2002) SIRT3, a human SIR2 homologue, is an NAD-dependent deacetylase localized to mitochondria, *Proc. Natl. Acad. Sci. U.S.A. 99*, 13653−13658.
26. Schwer, B., North, B. J., Frye, R. A., Ott, M., and Verdin, E. (2002) The human silent information regulator (Sir)2 homologue hSIRT3 is a mitochondrial nicotinamide adenine dinucleotide-dependent deacetylase, *J. Cell Biol. 158*, 647−657.
27. Liszt, G., Ford, E., Kurtev, M., and Guarente, L. (2005) Mouse Sir2 homolog SIRT6 is a nuclear ADP-ribosyltransferase, *J. Biol. Chem. 280*, 21313−21320.
28. Tanner, K. G., Landry, J., Sternglanz, R., and Denu, J. M. (2000) Silent information regulator 2 family of NAD-dependent histone/protein deacetylases generates a unique product, 1-*O*-acetyl-ADP-ribose, *Proc. Natl. Acad. Sci. U.S.A. 97*, 14178−14182.
29. Sauve, A. A., Celic, I., Avalos, J., Deng, H., Boeke, J. D., and Schramm, V. L. (2001) Chemistry of gene silencing: the mechanism of NAD^+-dependent deacetylation reactions, *Biochemistry 40*, 15456−15463.
30. Jackson, M. D., and Denu, J. M. (2002) Structural identification of 2′- and 3′-*O*-acetyl-ADP-ribose as novel metabolites derived from the Sir2 family of beta-NAD^+-dependent histone/protein deacetylases, *J. Biol. Chem. 277*, 18535−18544.
31. Gray, S. G., and Ekstrom, T. J. (2001) The human histone deacetylase family, *Exp. Cell Res. 262*, 75−83.
32. Denu, J. M. (2003) Linking chromatin function with metabolic networks: Sir2 family of NAD(+)-dependent deacetylases, *Trends Biochem. Sci. 28*, 41−48.
33. Borra, M. T., O'Neill, F. J., Jackson, M. D., Marshall, B., Verdin, E., Foltz, K. R., and Denu, J. M. (2002) Conserved enzymatic production and biological effect of *O*-acetyl-ADP-ribose by silent information regulator 2-like NAD^+-dependent deacetylases, *J. Biol. Chem. 277*, 12632−12641.
34. Rafty, L. A., Schmidt, M. T., Perraud, A. L., Scharenberg, A. M., and Denu, J. M. (2002) Analysis of *O*-acetyl-ADP-ribose as a target for Nudix ADP-ribose hydrolases, *J. Biol. Chem. 277*, 47114−47122.
35. Kustatscher, G., Hothorn, M., Pugieux, C., Scheffzek, K., and Ladurner, A. G. (2005) Splicing regulates NAD metabolite binding to histone macroH2A, *Nat. Struct. Mol. Biol. 12*, 624−625.
36. Liou, G. G., Tanny, J. C., Kruger, R. G., Walz, T., and Moazed, D. (2005) Assembly of the SIR complex and its regulation by *O*-acetyl-ADP-ribose, a product of NAD-dependent histone deacetylation, *Cell 121*, 515−527.
37. Borra, M. T., Langer, M. R., Slama, J. T., and Denu, J. M. (2004) Substrate specificity and kinetic mechanism of the Sir2 family of NAD^+-dependent histone/protein deacetylases, *Biochemistry 43*, 9877−9887.
38. Bitterman, K. J., Anderson, R. M., Cohen, H. Y., Latorre-Esteves, M., and Sinclair, D. A. (2002) Inhibition of silencing and accelerated aging by nicotinamide, a putative negative regulator of yeast sir2 and human SIRT1, *J. Biol. Chem. 277*, 45099−45107.
39. Jackson, M. D., Schmidt, M. T., Oppenheimer, N. J., and Denu, J. M. (2003) Mechanism of nicotinamide inhibition and transglycosidation by Sir2 histone/protein deacetylases, *J. Biol. Chem. 278*, 50985−50998.
40. Sauve, A. A., and Schramm, V. L. (2003) Sir2 regulation by nicotinamide results from switching between base exchange and deacetylation chemistry, *Biochemistry 42*, 9249−9256.
41. Bradford, M. M. (1976) A rapid and sensitive method for the quantitation of microgram quantities of protein utilizing the principle of protein-dye binding, *Anal. Biochem. 72*, 248−254.
42. Bodanszky, M. (1993) *Principles of Peptide Synthesis*, 2nd ed., Springer-Verlag, Germany.
43. Borra, M. T., and Denu, J. M. (2004) Quantitative assays for characterization of the Sir2 family of NAD(+)-dependent deacetylases, *Methods Enzymol. 376*, 171−187.
44. Murray, B. W., Padrique, E. S., Pinko, C., and McTigue, M. A. (2001) Mechanistic effects of autophosphorylation on receptor tyrosine kinase catalysis: enzymatic characterization of Tie2 and phospho-Tie2, *Biochemistry 40*, 10243−10253.
45. Tanny, J. C., and Moazed, D. (2001) Coupling of histone deacetylation to NAD breakdown by the yeast silencing protein Sir2: Evidence for acetyl transfer from substrate to an NAD breakdown product, *Proc. Natl. Acad. Sci. U.S.A. 98*, 415−420.
46. Oppenheimer, N. J. (1978) The stereospecificity of pig brain NAD-glycohydrolase-catalyzed methanolysis of NAD, *FEBS Lett. 94*, 368−370.
47. Min, J., Landry, J., Sternglanz, R., and Xu, R. M. (2001) Crystal structure of a SIR2 homolog-NAD complex, *Cell 105*, 269−279.
48. Chang, J. H., Kim, H. C., Hwang, K. Y., Lee, J. W., Jackson, S. P., Bell, S. D., and Cho, Y. (2002) Structural basis for the NAD-dependent deacetylase mechanism of Sir2, *J. Biol. Chem. 277*, 34489−34498.
49. Zhao, K., Chai, X., and Marmorstein, R. (2003) Structure of the yeast Hst2 protein deacetylase in ternary complex with 2′-*O*-acetyl ADP ribose and histone peptide, *Structure (Cambridge) 11*, 1403−1411.
50. Zhao, K., Harshaw, R., Chai, X., and Marmorstein, R. (2004) Structural basis for nicotinamide cleavage and ADP-ribose transfer by NAD(+)-dependent Sir2 histone/protein deacetylases, *Proc. Natl. Acad. Sci. U.S.A. 101*, 8563−8568.
51. Avalos, J. L., Boeke, J. D., and Wolberger, C. (2004) Structural basis for the mechanism and regulation of Sir2 enzymes, *Mol. Cell 13*, 639−648.
52. Avalos, J. L., Bever, K. M., and Wolberger, C. (2005) Mechanism of sirtuin inhibition by nicotinamide: altering the NAD(+) cosubstrate specificity of a Sir2 enzyme, *Mol. Cell 17*, 855−868.
53. Kramers, H. A. (1940) Brownian motion in a field of force and the diffusion model of chemical reactions, *Physica (The Hague) 7*, 284−304.
54. Brouwer, A. C., and Kirsch, J. F. (1982) Investigation of diffusion-limited rates of chymotrypsin reactions by viscosity variation, *Biochemistry 21*, 1302−1307.
55. Blacklow, S. C., Raines, R. T., Lim, W. A., Zamore, P. D., and Knowles, J. R. (1988) Triosephosphate isomerase catalysis is diffusion controlled. Appendix: Analysis of triose phosphate equilibria in aqueous solution by ^{31}P NMR, *Biochemistry 27*, 1158−1167.
56. Hardy, L. W., and Kirsch, J. F. (1984) Diffusion-limited component of reactions catalyzed by *Bacillus cereus* beta-lactamase I, *Biochemistry 23*, 1275−1282.
57. Kurz, L. C., Weitkamp, E., and Frieden, C. (1987) Adenosine deaminase: viscosity studies and the mechanism of binding of substrate and of ground- and transition-state analogue inhibitors, *Biochemistry 26*, 3027−3032.
58. Tarnus, C., Muller, H. M., and Schuber, F. (1988) Chemical evidence in favor of a stabilized oxocarbonium-ion intermediate in the NAD^+ glycohydrolase-catalyzed reactions, *Bioorg. Chem. 16*, 38−51.
59. Berthelier, V., Tixier, J. M., Muller-Steffner, H., Schuber, F., and Deterre, P. (1998) Human CD38 is an authentic NAD(P)+ glycohydrolase, *Biochem. J. 330* (Part 3), 1383−1390.

60. Johnson, R. W., Marschner, T. M., and Oppenheimer, N. J. (1988) Pyridine nucleotide chemistry. A new mechanism for the hydroxide-catalyzed hydrolysis of the nicotinamide-glycosyl bond, *J. Am. Chem. Soc*. *110*, 2257−2263.
61. Cakir-Kiefer, C., Muller-Steffner, H., and Schuber, F. (2000) Unifying mechanism for Aplysia ADP-ribosyl cyclase and CD38/NAD(+) glycohydrolases, *Biochem. J. 349*, 203−210.
62. Pascal, M., and Schuber, F. (1976) The stereochemistry of calf spleen NAD-glycohydrolase-catalyzed NAD methanolysis, *FEBS Lett. 66*, 107−109.
63. Muller-Steffner, H. M., Augustin, A., and Schuber, F. (1996) Mechanism of cyclization of pyridine nucleotides by bovine spleen NAD^+ glycohydrolase, *J. Biol. Chem. 271*, 23967−23972.
64. Yost, D. A., and Anderson, B. M. (1983) Adenosine diphosphoribose transfer reactions catalyzed by Bungarus fasciatus venom NAD glycohydrolase, *J. Biol. Chem. 258*, 3075−3080.
65. Sauve, A. A., Munshi, C., Lee, H. C., and Schramm, V. L. (1998) The reaction mechanism for CD38. A single intermediate is responsible for cyclization, hydrolysis, and base-exchange chemistries, *Biochemistry 37*, 13239−13249.
66. Tanny, J. C., Dowd, G. J., Huang, J., Hilz, H., and Moazed, D. (1999) An enzymatic activity in the yeast Sir2 protein that is essential for gene silencing, *Cell 99*, 735−745.
67. Garcia-Salcedo, J. A., Gijon, P., Nolan, D. P., Tebabi, P., and Pays, E. (2003) A chromosomal SIR2 homologue with both histone NAD-dependent ADP-ribosyltransferase and deacetylase activities is involved in DNA repair in *Trypanosoma brucei*, *EMBO J. 22*, 5851−5862.
68. Denu, J. M. (2005) The Sir2 family of protein deacetylases, *Curr. Opin. Chem. Biol. 9*, 431−440.
69. Sauve, A. A., Deng, H., Angeletti, R. H., and Schramm, V. L. (2000) A covalent intermediate in CD38 is responsible for ADP-ribosylation and cyclization reactions, *J. Am. Chem. Soc. 122*, 7855−7859.

BI052014T